
SIGMA: Structure-Invariant Generative Molecular Alignment for Chemical Language Models via Autoregressive Contrastive Learning

Xinyu Wang¹ Fei Dou² Jinbo Bi¹ Minghu Song³

Abstract

Linearized string representations serve as the foundation of scalable autoregressive molecular generation; however, they introduce a fundamental modality mismatch where a single molecular graph maps to multiple distinct sequences. This ambiguity leads to *trajectory divergence*, where the latent representations of structurally equivalent partial graphs drift apart due to differences in linearization history. To resolve this without abandoning the efficient string formulation, we propose **Structure-Invariant Generative Molecular Alignment (SIGMA)**. Rather than altering the linear representation, SIGMA enables the model to strictly recognize geometric symmetries via a token-level contrastive objective, which explicitly aligns the latent states of prefixes that share identical suffixes. Furthermore, we introduce **Isomorphic Beam Search (IsoBeam)** to eliminate isomorphic redundancy during inference by dynamically pruning equivalent paths. Empirical evaluations on standard benchmarks demonstrate that SIGMA bridges the gap between sequence scalability and graph fidelity, yielding superior sample efficiency and structural diversity in multi-parameter optimization compared to strong baselines.

1. Introduction

Drug discovery has been fundamentally reshaped by Chemical Language Models (ChemLMs), which cast molecular design as a sequence modeling problem (Chithrananda et al., 2020; Bran et al., 2023; Bagal et al., 2021; Li et al., 2023). This paradigm parallels the success of Large Language Models (LLMs), where scaling Transformer architec-

tures (Vaswani et al., 2017) enables modeling of complex linguistic dependencies (Devlin et al., 2019; Radford et al., 2019; Liu et al., 2019; Jiang et al., 2023). Inspired by this progress, cheminformatics has adopted self-attention mechanisms under the assumption that chemical connectivity rules can be learned analogously to linguistic grammar.

To enable this linguistic processing, molecular graphs are typically serialized into 1D string representations, with the Simplified Molecular Input Line Entry System (SMILES) being the *de facto* standard (Weininger, 1988). This linearization allows models to leverage vast, unlabelled chemical repositories for pre-training, drawing from massive databases such as PubChem (Wang et al., 2009), ChEMBL (Gaulton et al., 2012), and ZINC (Irwin & Shoichet, 2005; Sterling & Irwin, 2015). By estimating probability distributions over these molecular strings, ChemLMs have achieved significant breakthroughs across a spectrum of downstream applications. These range from the *de novo* generation of novel drug candidates (Xu et al., 2024; Lee et al., 2024) to the precise prediction of molecular properties (Wang et al., 2019; Honda et al., 2019) and complex bioactivity modeling (Seal et al., 2022; 2023).

However, treating chemistry as language introduces a fundamental modality mismatch between 1D sequences and the underlying 2D/3D molecular graph. Unlike natural language, where word order is semantic, molecular serialization order is arbitrary. A single graph can correspond to factorially many valid SMILES strings depending on traversal choices. Standard autoregressive models, lacking geometric inductive biases of Message Passing Neural Networks (MPNNs) (Gilmer et al., 2017; Hu et al., 2019), treat these permutations as distinct sequences. Alternative encodings such as SELFIES (Krenn et al., 2020) and DeepSMILES (O’Boyle & Dalke, 2018) improve robustness but do not eliminate the one-to-many mapping issue (Scalia et al., 2020; Gao et al., 2022). As illustrated in Figure 1 (and Appendix A), this causes *trajectory divergence*: two equivalent partial molecular graphs can follow different linearization paths and drift apart in latent space.

This divergence leads to **manifold fragmentation**, where chemical space splits into clusters defined by syntax rather than structure. For optimization, this is harmful: reinforce-

¹School of Computing, University of Connecticut, Storrs, CT, USA ²Institute for Artificial Intelligence, University of Georgia, Athens, GA, USA ³Institute of Hydrobiology, Chinese Academy of Sciences, Wuhan, China.

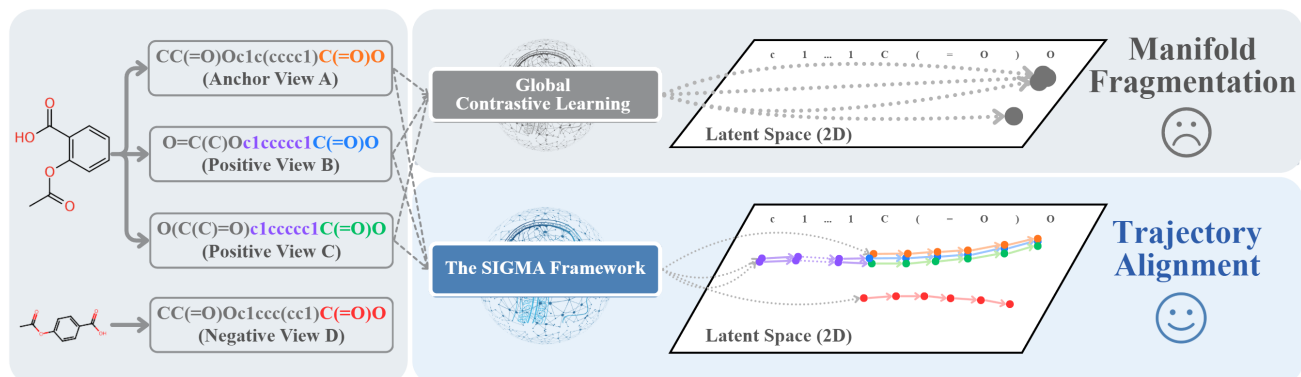


Figure 1. Conceptual comparison between Global Contrastive Learning and our proposed Structure-Invariant Autoregressive Contrastive Learning (SIGMA). Top: Traditional methods treat different SMILES permutations (Views A, B, C) of the same molecule as distinct sequences, and only contrast the complete SMILES strings, causing Manifold Fragmentation where functionally equivalent states (substrings) map to disparate points in the latent space. Bottom: SIGMA enforces Trajectory Alignment. By identifying that Views A, B, and C share a topologically identical suffix, SIGMA explicitly aligns their generation paths into a unified trajectory, while pushing away structurally distinct negative samples (View D).

ment learning agents may remain confined to one syntactic region, limiting exploration and inducing mode collapse. Existing remedies rely on Randomized SMILES augmentation (Bjerrum, 2017) or auxiliary graph encoders (Zhu et al., 2023), assuming invariance emerges from exposure. In practice, models often memorize frequent permutations instead of learning structural equivalence, yielding poor sample efficiency (Tetko et al., 2020). Graph-based generators (Wang et al., 2025) encode geometry explicitly but sacrifice the scalability and stability of sequence Transformers. A framework is needed that preserves sequence efficiency while enforcing strict geometric invariance.

Therefore, we propose **Structural-Invariant Generative Molecular Alignment (SIGMA)** via autoregressive contrastive learning, a framework designed to resolve trajectory divergence by embedding geometric consistency directly into the autoregressive backbone. Instead of relying on passive data augmentation, SIGMA employs a rigorous token-level contrastive objective (shown in Figure 2). We construct pairs of randomized prefix trajectories that describe the same partial graph and share identical valid future completions. By aligning their latent representations, SIGMA reconnects fragmented regions of the latent manifold, enabling geometry-invariant understanding regardless of molecular syntax.

Furthermore, *trajectory invariance* can be incorporated into model training but should also be recognized during inference. Commonly used sampling methods, such as random sampling and beam search, frequently suffer from isomorphic redundancy, wasting computational resources by generating multiple SMILES strings that decode to the same molecule. To address this, we introduce **Isomorphic Beam Search (IsoBeam)**, a structure-aware decoding strategy shown in Figure 3. IsoBeam dynamically detects when different search paths converge to identical subgraphs and

prunes the redundant trajectories, reallocating the search budget to explore structurally distinct scaffolds.

Our main contributions are summarized as follows:

- We identify Manifold Fragmentation caused by trajectory divergence as the root cause of inefficiency in ChemLMs. We propose SIGMA to enforce latent isotropy via dense trajectory alignment, effectively making the sequence model behave like a graph model in latent space.
- We introduce a novel Structure-Invariant Contrastive Loss that operates at the token level during the generation of the SMILES. By maximizing the mutual information between equivalent generation paths, we decouple chemical semantics from syntactic variation.
- We propose IsoBeam, an inference algorithm that eliminates isomorphic redundancy. Empirical results demonstrate that IsoBeam significantly increases the structural diversity of generated molecules.

2. Related Work

Generative Models for Molecular Design. Deep generative models for molecules broadly fall into two categories: graph-based and sequence-based approaches. Graph generative models, such as GCPN (You et al., 2018), GraphAF (Shi et al., 2020), and LO-ARM (Wang et al., 2025), construct molecules node-by-node or via motif assembly. These models possess intrinsic permutation invariance but typically rely on complex graph matching operations or expensive validity masking, limiting their scalability.

In contrast, ChemLMs leverage the efficiency of Transformer architectures to process molecules as linearized SMILES strings (Bagal et al., 2021; Chithrananda et al.,

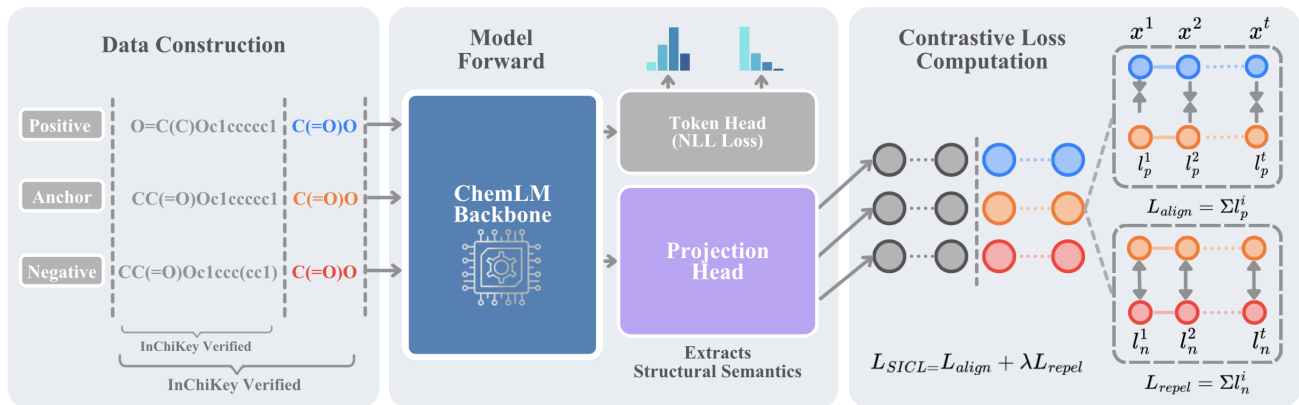


Figure 2. Token-level contrastive supervision across equivalent SMILES sequences. Two structurally equivalent SMILES (top: constrained random, bottom: original) are decoded independently using an autoregressive model. Positive alignment losses (suffix-align) are applied over matched suffix tokens (shown in blue and green), while negative repulsion (prefix-repel) is enforced between mismatched prefix tokens (in red). (Left) Token distribution alignment is computed using output logits; (Right) attention alignment compares cross-attention weights across matched positions.

2020). While ChemLMs scale effectively, they suffer from a modality mismatch: the linearization process destroys topological locality. Recent benchmarks indicate that this lack of geometric inductive bias leads to brittle representations, where semantically equivalent but syntactically distinct SMILES elicit inconsistent behaviors (Ganeeva et al., 2024). Our work aims to fill this gap, inducing the geometric rigor of graph models into the scalable architecture of ChemLMs via structural alignment.

Canonicalization Bias and Data Augmentation. The many-to-one mapping from molecular graphs to SMILES strings creates isomorphic ambiguity (Weininger, 1988). This canonicalization bias arises when models memorize the rigid syntax of canonical SMILES rather than the underlying molecular geometry. The prevalent mitigation strategy is data augmentation via Randomized SMILES (Bjerrum, 2017; Ar-Pous et al., 2019). While augmentation improves robustness, naive enumeration fails to cover the full syntactic manifold due to combinatorial explosion (Tetko et al., 2020). As a result, models often memorize specific fragments rather than learning a generalized invariant mapping. Unlike these implicit approaches, SIGMA explicitly enforces invariance through a structured contrastive objective, decoupling geometric learning from the combinatorial explosion of string enumeration.

Contrastive Learning in Molecular Representation. *Global Alignment.* Early methods aligned global representations. Graph-based approaches (e.g., MolCLR (Wang et al., 2022)) maximize agreement between perturbed graphs. In the sequence domain, SimSon (Pinheiro et al., 2022) and CONSMI (Qian et al., 2024) adapt SimCLR to align global SMILES embeddings (e.g., [CLS] token). While CONSMI conditions generation on invariant latents, its coarse-grained alignment is insufficient for guiding the fine-grained,

step-by-step decisions required in autoregressive decoding (Fabian et al., 2020).

Token-level Alignment. To enable fine-grained control, token-wise approaches have emerged. In NLP, SimCTG (Su et al., 2021) uses self-contrastive loss to reduce anisotropy, forcing intra-sequence token distinctiveness to prevent degeneration. However, it lacks inter-sequence structural alignment. Molecular adaptations like FineMolTex (Zhou et al., 2024) align tokens with motifs but often necessitate complex multi-modal architectures.

SIGMA bridges these paradigms via **Dense Trajectory Alignment**. Unlike SimCTG (intra-sequence) or SimSon (global), SIGMA aligns token-level trajectories *across* structurally equivalent views. By contrasting shared suffixes against structurally distinct negatives, it ensures generative dynamics strictly adhere to the underlying chemical topology.

3. Methodology

The proposed SIGMA is a framework designed to resolve the modality mismatch in autoregressive ChemLMs. Unlike standard approaches that treat SMILES permutations as independent sequences, SIGMA enforces geometric isotropy in the latent space by explicitly aligning the generative trajectories of structurally equivalent molecular views.

3.1. Problem Formulation: Generative Modeling on Chemical Manifolds

Let $\mathcal{G} \in \mathbb{G}$ be a molecular graph defined by a set of atoms and bonds. In the context of autoregressive modeling, \mathcal{G} is serialized into a sequence of tokens $S = (x_1, \dots, x_L)$ from a vocabulary \mathcal{V} . A fundamental challenge in this domain is the *one-to-many* mapping: a single graph \mathcal{G} corresponds

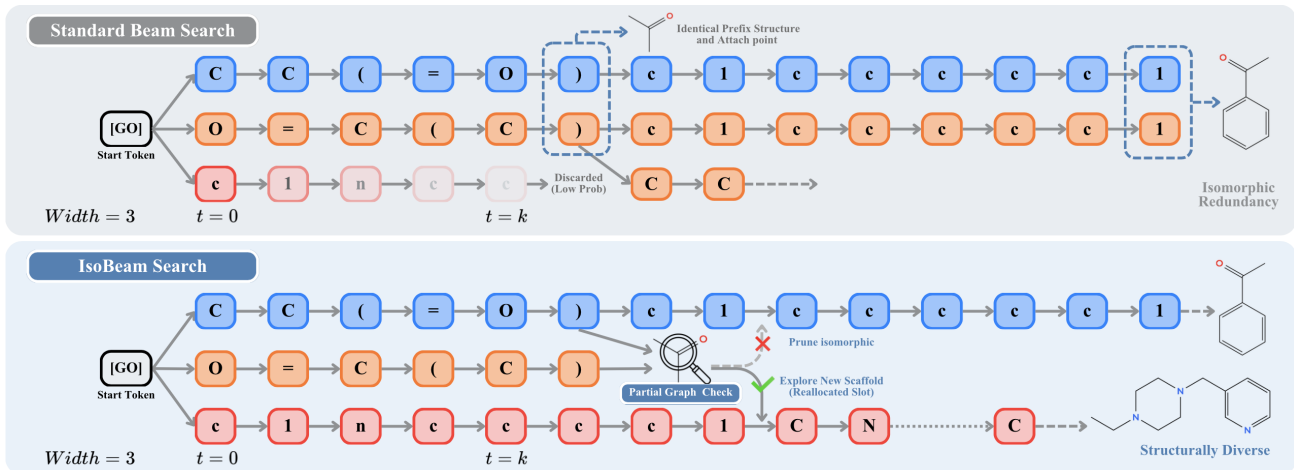


Figure 3. Resolving Isomorphic Redundancy with Isomorphic Beam (IsoBeam) Search. (Top) Standard Beam Search: Beam capacity is wasted on multiple linearizations of the same molecule (e.g., variants of acetophenone), causing isomorphic redundancy where topologically identical duplicates crowd the search space. (Bottom) IsoBeam Search: A Partial Graph Check verifies if prefixes share identical substructures and consistent attachment points. Lower-probability isomorphic paths are dynamically pruned (red cross), reallocating the budget to explore distinct trajectories (e.g., a pyridine-based scaffold), thereby maximizing structural diversity.

to a factorial set of valid SMILES permutations $\Pi(\mathcal{G}) = \{S^{(1)}, \dots, S^{(K)}\}$, determined by the traversal order.

Standard ChemLMs maximize the likelihood of a sequence S via the autoregressive factorization:

$$\log p_{\theta}(S) = \sum_{t=1}^L \log p_{\theta}(x_t | x_{<t}) \quad (1)$$

While effective for unique sequences (e.g., natural language), this objective treats $S^{(i)}$ and $S^{(j)}$ from the same equivalence class $\Pi(\mathcal{G})$ as distinct, unrelated training examples. This leads to *Trajectory Divergence*: the hidden states $h_t(S^{(i)})$ and $h_t(S^{(j)})$ corresponding to the same chemical substructure are mapped to orthogonal regions in the latent manifold. Our goal is to learn a parameterized encoder $f_{\theta}(\cdot)$ such that the latent representations remain invariant under the permutation group of the graph:

$$f_{\theta}(x_{<t}^{(i)}) \approx f_{\theta}(x_{<t}^{(j)}) \quad \text{if} \quad \text{Mol}(x_{<t}^{(i)}) \cong \text{Mol}(x_{<t}^{(j)}) \quad (2)$$

where \cong denotes subgraph isomorphism.

3.2. Constructing Functionally Equivalent Views

A critical prerequisite for contrastive learning is the rigorous identification of positive pairs. Naive augmentation often leads to *syntactic false positives*—prefixes that map to isomorphic subgraphs but are syntactically incompatible (e.g., one expecting a ring-closure digit, the other a branch opening). To address this, we propose a view construction pipeline rooted in *Functional Equivalence*.

We construct a positive pair (S^u, S^v) by sampling two randomized traversals that diverge in their history but converge to a common future trajectory. Formally, we decompose the generation process into a prefix p and a suffix s . We aim

to find two distinct prefixes p_u and p_v that are compatible with the *exact same* suffix string s . The validity of the pair (p_u, p_v) is conditioned on the **Dual Consistency Condition**:

- Syntactic Divergence** ($p_u \neq p_v$): The prefixes must represent distinct graph traversal histories (e.g., starting from different atoms or traversing branches in reverse orders), ensuring the contrastive task is non-trivial.
- Structural Equivalence via Oracle Verification**: The concatenation of both prefixes with the shared suffix s must reconstruct the identical molecular graph \mathcal{G} . We verify this using the InChIKey hashing oracle \mathcal{H} :

$$\mathcal{H}(\text{Mol}(p_u \oplus s)) \equiv \mathcal{H}(\text{Mol}(p_v \oplus s)) \equiv \mathcal{H}(\mathcal{G}) \quad (3)$$

The ‘Probe Suffix’ Protocol. A practical engineering challenge is that incomplete SMILES prefixes are often chemically invalid and cannot be processed by standard informatics tools. To resolve this, we employ a **Probe Suffix Protocol**. During training view construction, if a random split point leaves open rings or unclosed branches, we temporarily append a chemically stable completion fragment s_{probe} (e.g., a methyl cap or ring closure) solely for the purpose of structure verification. This ensures that the equivalence is based on the rigid topological structure rather than unstable transient states.

Structural Negatives. Standard contrastive methods often rely on random in-batch negatives. However, this is insufficient for fine-grained chemical discrimination. We introduce **Structural Negatives**: for a given anchor prefix p_u , we explicitly sample a negative prefix p_{neg} from the batch such that $\mathcal{H}(\text{Mol}(p_{neg} \oplus s)) \neq \mathcal{H}(\mathcal{G})$. This forces

the model to distinguish between truly isomorphic trajectories and those representing distinct chemical entities (e.g., stereoisomers or scaffold hops), sharpening the decision boundary in the latent space.

3.3. Architecture and Parameterization

We instantiate our framework using a autoregressive architecture. Let f_θ denote the backbone network parameterized by θ . Given a SMILES sequence S , the model computes a sequence of contextual hidden states $\mathbf{H} = [\mathbf{h}_1, \dots, \mathbf{h}_L]$, where $\mathbf{h}_t \in \mathbb{R}^{d_{model}}$.

Projection-Decoupled Mechanism. Directly applying contrastive loss on the backbone representations \mathbf{H} restricts the expressivity required for the primary generative task. The MLE objective relies on precise syntactic features (e.g., specific ring indices ‘1’ vs ‘2’) to predict the next token, whereas contrastive learning seeks to abstract away from these superficial variations. To resolve this **Syntax-Semantics Conflict**, we introduce a dedicated non-linear **Projection Head** g_ϕ mapping \mathbf{H} to a lower-dimensional metric space \mathcal{Z} :

$$\mathbf{z}_t = g_\phi(\mathbf{h}_t) = W^{(2)}\sigma(W^{(1)}\mathbf{h}_t + b^{(1)}) + b^{(2)} \quad (4)$$

where σ is a ReLU activation, $W^{(1)} \in \mathbb{R}^{d_{model} \times d_{model}}$, and $W^{(2)} \in \mathbb{R}^{d_{proj} \times d_{model}}$. In our implementation, we set $d_{model} = 768$ and $d_{proj} = 128$. This bottleneck architecture acts as an information filter, preserving only the essential structural semantics required for the invariance objective, while the backbone \mathbf{h}_t retains the full syntactic context for autoregressive prediction.

Siamese Forward Pass. During training, the model operates in a Siamese manner with shared weights. For a given mini-batch of N molecules, we generate $2N$ augmented views (functionally equivalent pairs). These are processed in parallel to obtain the representations \mathbf{Z}_u and \mathbf{Z}_v . The autoregressive loss \mathcal{L}_{MLE} is computed on the logits derived from \mathbf{H} (ensuring syntactic validity), while the structural regularization \mathcal{L}_{SIGMA} is computed on the normalized projections $\hat{\mathbf{z}} = \mathbf{z}/\|\mathbf{z}\|_2$ (ensuring geometric consistency).

3.4. Dense Trajectory Alignment Objective

Previous works in molecular contrastive learning typically employ *Global Alignment* (e.g., aligning [CLS] tokens). However, autoregressive generation is a sequential decision process where errors can accumulate. To enforce fine-grained consistency, we propose a **Dense Trajectory Alignment** objective.

Formulation. Consider the projected embeddings of the suffix tokens for a positive pair, denoted as \mathbf{Z}_{suf}^u and \mathbf{Z}_{suf}^v ,

Algorithm 1 Isomorphic Beam Search (IsoBeam)

Require: Beam size K , Model \mathcal{M} , Oracle \mathcal{H} (e.g., RDKit to InChIKey)

- 1: Initialize Beam $\mathcal{B} \leftarrow \{[\text{BOS}]\}$
- 2: **for** $t = 1 \dots T_{\max}$ **do**
- 3: Expand \mathcal{B} to candidates via top- k sampling
- 4: $\mathcal{B}_{new} \leftarrow \emptyset, \mathcal{S}_{seen} \leftarrow \emptyset$
- 5: Sort candidates by cumulative log-probability
- 6: **for** each candidate c in candidates **do**
- 7: $M \leftarrow \text{MolFromSmiles}(c)$
- 8: **if** M is **None** **then**
- 9: // Keep invalid intermediates for completion
- 10: $\mathcal{B}_{new} \leftarrow \mathcal{B}_{new} \cup \{c\}$
- 11: **else**
- 12: // Check structural uniqueness for valid graphs
- 13: $id \leftarrow \mathcal{H}(M)$
- 14: **if** $id \notin \mathcal{S}_{seen}$ **then**
- 15: $\mathcal{B}_{new} \leftarrow \mathcal{B}_{new} \cup \{c\}$
- 16: $\mathcal{S}_{seen} \leftarrow \mathcal{S}_{seen} \cup \{id\}$
- 17: **end if**
- 18: **end if**
- 19: **if** $|\mathcal{B}_{new}| = K$ **then**
- 20: **break**
- 21: **end if**
- 22: **end for**
- 23: $\mathcal{B} \leftarrow \mathcal{B}_{new}$
- 24: **end for**
- 25: **Output:** \mathcal{B}

and a set of structural negatives. We compute the token-wise similarity matrix between the trajectories. The goal is to maximize the likelihood that the t -th token in the suffix of view u aligns with the corresponding t -th token in view v . The loss for a specific time step t in the suffix is formulated as:

$$\mathcal{L}_{SIGMA}^{(t)} = -\log \frac{\exp(\text{sim}(\mathbf{z}_{u,t}, \mathbf{z}_{v,t})/\tau)}{\exp(\text{sim}(\mathbf{z}_{u,t}, \mathbf{z}_{v,t})/\tau) + \sum_{k \in \mathcal{N}_{neg}} \exp(\text{sim}(\mathbf{z}_{u,t}, \mathbf{z}_{k,t})/\tau)} \quad (5)$$

where $\text{sim}(\cdot, \cdot)$ denotes cosine similarity and τ is a temperature parameter. Crucially, rather than aligning a single pivot point, we average this objective over the entire suffix length L_{suf} :

$$\mathcal{L}_{SIGMA} = \frac{1}{L_{suf}} \sum_{t=1}^{L_{suf}} \mathcal{L}_{SIGMA}^{(t)} \quad (6)$$

Theoretical Insight: Implicit Gradient Alignment. A key theoretical question is: why does aligning the *suffix* representations enforce invariance in the *prefix* representations? We analyze this through the lens of gradient flow. In a causal Transformer, the hidden state of a suffix token s_t is a function of the prefix context p and the preceding suffix tokens $s_{<t}$: $\mathbf{h}_{s_t} = \text{Transformer}(s_t | p, s_{<t})$. In our construction, for a positive pair, the suffix inputs $s_{<t}$ are identical. The only variable is the prefix p . Minimizing the contrastive loss \mathcal{L}_{SIGMA} between $\mathbf{h}_{s_t}^u$ and $\mathbf{h}_{s_t}^v$ necessitates minimizing the distance between the conditional distributions induced by

p_u and p_v . Since the suffix parameters are shared, the gradient $\nabla \mathcal{L}_{SIGMA}$ backpropagates through the suffix attention layers to update the prefix encoder, effectively enforcing:

$$\text{Encoder}(p_u) \approx \text{Encoder}(p_v) \quad (7)$$

Thus, dense trajectory alignment acts as a robust proxy for aligning the prefix representations, leveraging the causal structure of the model to propagate invariance backwards from the future (suffix) to the past (prefix).

The final training objective combines the generative and contrastive tasks: $\mathcal{L}_{total} = \mathcal{L}_{NLL} + \lambda \mathcal{L}_{SIGMA}$, where λ is a hyperparameter balancing generation quality and structural regularization.

3.5. Isomorphic Beam Search (IsoBeam)

While SIGMA aligns the latent space during training, standard Beam Search allows the generation of redundant syntactic variations during inference. To address this, we introduce **IsoBeam**, which enforces structural uniqueness dynamically.

The core mechanism of IsoBeam is to prune candidates that correspond to already-visited molecular graphs. At each decoding step t , for every candidate sequence c in the beam:

1. **Validity Check:** We first check if the current partial sequence c forms a syntactically valid molecule (e.g., using RDKit).
2. **Conditional Pruning:** If c is **invalid** (e.g., open rings or branches), it is retained in the beam to allow for future completion. If c is **valid**, we compute its structural identifier (InChIKey). If this identifier has already been encountered in the current beam (meaning it is an isomorphic variant of a higher-probability candidate), c is pruned. Otherwise, it is retained and its identifier is added to the visited set.

This strategy ensures that the beam does not waste capacity on multiple permutations of the same valid substructure or molecule, effectively maximizing the exploration of unique chemical space.

Complexity vs. Diversity Trade-off. Although IsoBeam introduces an overhead for RDKit validation at each step, it dramatically increases the *effective beam size*. In standard beam search, a beam of size $K = 10$ might contain only 2 unique molecular structures (with 5 permutations each). In IsoBeam, a beam of size $K = 10$ is guaranteed to contain 10 topologically distinct structures. This trade-off is highly favorable for molecular optimization tasks where sample efficiency and scaffold diversity are paramount.

4. Experiments

Experimental Setup We evaluate SIGMA on unsupervised molecular generation and goal-directed optimization. The backbone is a GPT-2 (Small) causal language model trained on **ZINC-250k** (Irwin & Shoichet, 2005). Baselines include: (1) *Sequence Models*, trained on canonical SMILES or randomized SMILES augmentation (*RandAugment*); (2) *Graph-based SOTA*, namely LO-ARM (Wang et al., 2025); and (3) *Ablations* without the dense contrastive objective. Full implementation and hyperparameters are in Appendix B.

4.1. Analysis of Geometric Invariance

A central hypothesis of this work is that standard autoregressive objectives lead to *manifold fragmentation*, whereas SIGMA enforces a smooth, geometry-invariant latent space. We verify this through macroscopic visualization, microscopic alignment analysis, and quantitative consistency metrics.

Macroscopic: Resolving Manifold Fragmentation. We sample 10 molecules and generate 50 randomized SMILES views each. Terminal hidden states are projected via t-SNE. As shown in Fig. 4, the baseline latent space is entangled, with isomorphic views scattered. Data augmentation improves separation but still produces fragmented clusters. SIGMA collapses all permutations of a molecule into compact, well-separated clusters, indicating successful abstraction from syntactic variation.

Microscopic: Isomorphic Semantic Alignment. We analyze token-level representations using cosine similarity between hidden states of two equivalent but differently serialized trajectories of Acetophenone (Fig. 5). Baselines show alignment only along identical suffix tokens. SIGMA exhibits a clear off-diagonal semantic block, demonstrating alignment of equivalent chemical substructures despite different character sequences. This shows SIGMA learns structural semantics rather than memorizing syntax.

4.2. Unconditional Generation: Bridging Sequence and Graph Models

We next investigate whether the learned geometric invariance translates to superior generative quality on the ZINC-250k benchmark. Historically, a trade-off exists in generative chemistry: sequence models achieve high validity but suffer from distribution shift (high Fréchet ChemNet Distance, FCD), while graph models capture the distribution well but often struggle with validity constraints.

As presented in Table 2, SIGMA effectively bridges this gap.

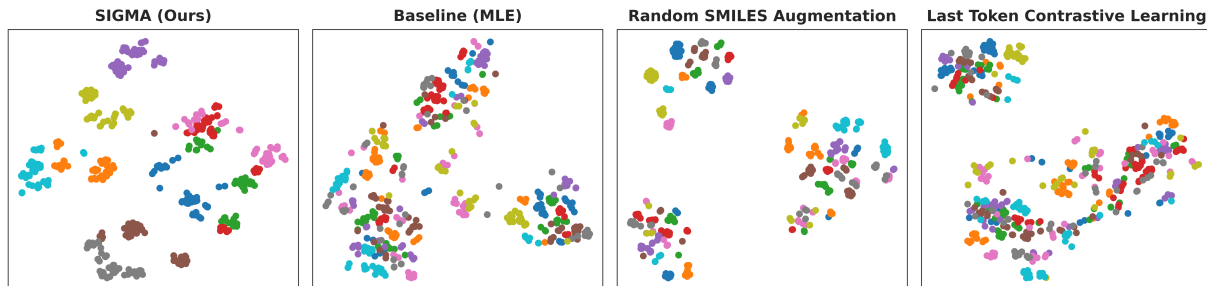


Figure 4. Latent Space Visualization of Geometric Invariance. We utilize t-SNE to project the terminal hidden states of 50 randomized SMILES views for 10 distinct molecules (color-coded by molecular identity). **SIGMA (Ours)** achieves superior geometric invariance, where isomorphic views collapse into tight, well-separated clusters. In contrast, the **Baseline (MLE)** exhibits severe *manifold fragmentation*, with isomorphic trajectories scattered and entangled. **Random SMILES Augmentation** improves separation but suffers from disconnected islands, where a single molecule maps to multiple disjoint clusters. **Last Token Contrastive Learning** fails to cleanly disentangle structural identities, demonstrating that dense token-level alignment is essential for learning isotropic representations.

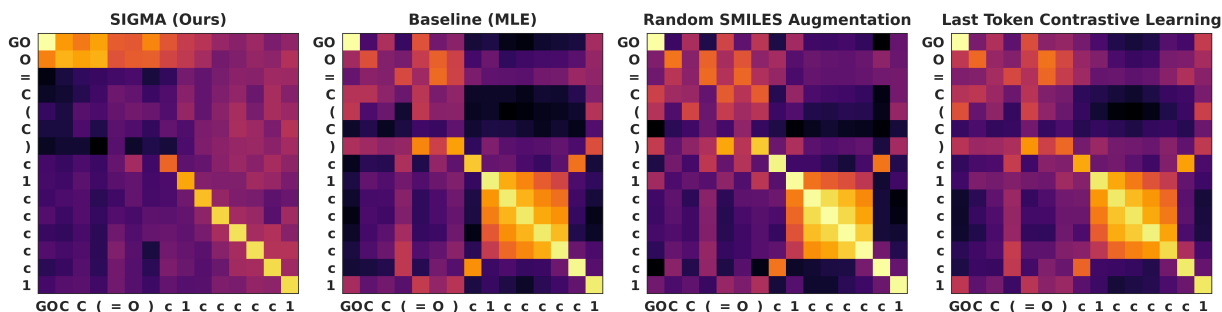


Figure 5. Token-wise Latent Alignment Heatmaps. We visualize the cosine similarity matrices of hidden states between two syntactically distinct SMILES linearizations of Acetophenone (y-axis: CC(=O) . . . , x-axis: O=C(C) . . .). **SIGMA (Left)** exhibits a distinct **semantic alignment block** in the top-left region. Despite the disjoint syntax of the prefix (acetyl group), the model aligns the latent representations of CC(=O) and O=C(C), confirming it captures the underlying structural equivalence. In contrast, the **Baseline** and **GCL** models show near-zero similarity (dark blue) in this off-diagonal region, indicating they rely primarily on surface-level token matching and fail to recognize the structural identity of the permuted prefixes. All models successfully align the identical suffix (c1ccccc1, bottom-right diagonal).

- **Validity & Uniqueness:** SIGMA maintains the near-perfect validity ($> 99.8\%$) characteristic of autoregressive sequence models, significantly outperforming graph-based baselines like GraphAF and MoFlow.
- **Distributional Fidelity (FCD):** Crucially, SIGMA achieves a Fréchet ChemNet Distance (FCD) of **0.752**. This is not only a substantial improvement over the standard sequence baselines (e.g., CharRNN: 0.965, RandSMILES: 0.892) but also establishes a new state-of-the-art among sequence-based methods.

This result confirms that by resolving manifold fragmentation, SIGMA learns a chemical probability distribution that is both syntactically robust (high validity) and chemically realistic (low FCD), effectively competing with computationally expensive graph autoregressive models (e.g., LO-ARM).

4.3. Optimization Efficiency in Reinforcement Learning

To rigorously assess if SIGMA’s geometric invariance improves optimizability, we adopt a **plug-and-play protocol** using the standard REINVENT algorithm (Olivecrona et al., 2017) as a fixed backbone. This design isolates the quality of the generative prior as the sole variable affecting performance. We evaluate on the PMO Benchmark (MPO and exploration tasks), with results summarized in Table 1.

Regarding raw optimization, SIGMA performs comparably to the baseline, an expected outcome due to RL-driven score saturation. However, a critical divergence appears in structural diversity. SIGMA generates significantly more unique scaffolds (#Scaf) across all tasks. For instance, in the Osimertinib task, SIGMA identifies over **7,700 unique scaffolds** a $\sim 40\%$ increase over the baseline (5,600) despite achieving similar peak scores.

This highlights distinct exploration dynamics. While the baseline suffers from mode collapse (generating trivial vari-

Table 1. **PMO Benchmark Performance.** (mean \pm s.d. over 3 runs). Blue and pink shading indicate superior performance by SIGMA and the baseline, respectively. While peak scores (Top-1, Avg-100) are comparable due to saturation, **SIGMA significantly excels in exploration (#Scaf).** In tasks like Osimertinib, SIGMA discovers 20–40% more unique scaffolds, confirming that geometric invariance facilitates effective *scaffold hopping* rather than local exploitation.

Task	Use SIGMA	Optimization Quality			Efficiency			SA (†)	Exploration Div (†)	# Scaf (†)
		Top-Avg 1 (†)	Tio-Avg 10 (†)	Top-Avg 100 (†)	Top-AUC 1 (†)	Top-AUC 10 (†)	Top-AUC 100 (†)			
MPO (Multiproperty Objective)										
Sitagliptin	-	0.552 \pm 0.029	0.540 \pm 0.035	0.498 \pm 0.032	0.502 \pm 0.050	0.473 \pm 0.034	0.404 \pm 0.040	2.823 \pm 0.356	0.603 \pm 0.091	2670 \pm 489
	✓	0.607 \pm 0.013	0.596 \pm 0.020	0.541 \pm 0.014	0.544 \pm 0.011	0.508 \pm 0.020	0.423 \pm 0.016	3.628 \pm 0.487	0.656 \pm 0.073	3143 \pm 89
Zaleplon	-	0.616 \pm 0.040	0.611 \pm 0.037	0.593 \pm 0.031	0.557 \pm 0.011	0.535 \pm 0.006	0.493 \pm 0.007	2.400 \pm 0.247	0.479 \pm 0.083	3518 \pm 441
	✓	0.635 \pm 0.015	0.627 \pm 0.016	0.610 \pm 0.013	0.578 \pm 0.007	0.558 \pm 0.005	0.517 \pm 0.002	2.833 \pm 0.046	0.531 \pm 0.035	3902 \pm 298
Fexofenadine	-	0.893 \pm 0.012	0.889 \pm 0.014	0.877 \pm 0.020	0.794 \pm 0.017	0.776 \pm 0.016	0.745 \pm 0.015	4.525 \pm 0.211	0.444 \pm 0.011	6211 \pm 412
	✓	0.957 \pm 0.023	0.945 \pm 0.023	0.932 \pm 0.020	0.807 \pm 0.006	0.790 \pm 0.005	0.758 \pm 0.004	4.360 \pm 0.423	0.376 \pm 0.059	6272 \pm 467
Osimertinib	-	0.910 \pm 0.021	0.906 \pm 0.022	0.896 \pm 0.019	0.847 \pm 0.008	0.835 \pm 0.008	0.807 \pm 0.007	3.476 \pm 0.257	0.463 \pm 0.063	5667 \pm 941
	✓	0.902 \pm 0.003	0.899 \pm 0.004	0.892 \pm 0.002	0.846 \pm 0.004	0.836 \pm 0.003	0.808 \pm 0.003	3.460 \pm 0.154	0.532 \pm 0.039	7731 \pm 190
Perindopril	-	0.642 \pm 0.047	0.642 \pm 0.047	0.639 \pm 0.057	0.550 \pm 0.026	0.536 \pm 0.023	0.512 \pm 0.017	4.245 \pm 0.249	0.340 \pm 0.084	5295 \pm 317
	✓	0.648 \pm 0.005	0.647 \pm 0.006	0.643 \pm 0.006	0.552 \pm 0.003	0.539 \pm 0.002	0.514 \pm 0.001	4.383 \pm 0.163	0.405 \pm 0.093	6188 \pm 263
Median Molecule										
Median 1	-	0.417 \pm 0.024	0.417 \pm 0.024	0.407 \pm 0.029	0.372 \pm 0.016	0.365 \pm 0.016	0.341 \pm 0.018	4.748 \pm 0.428	0.298 \pm 0.115	1618 \pm 334
	✓	0.431 \pm 0.018	0.431 \pm 0.018	0.415 \pm 0.011	0.393 \pm 0.014	0.385 \pm 0.014	0.359 \pm 0.012	4.922 \pm 0.144	0.458 \pm 0.047	1692 \pm 161
Median 2	-	0.349 \pm 0.012	0.342 \pm 0.011	0.329 \pm 0.007	0.299 \pm 0.009	0.285 \pm 0.004	0.265 \pm 0.003	2.953 \pm 0.314	0.412 \pm 0.014	5654 \pm 201
	✓	0.346 \pm 0.002	0.335 \pm 0.004	0.323 \pm 0.003	0.304 \pm 0.003	0.287 \pm 0.002	0.265 \pm 0.001	2.785 \pm 0.138	0.397 \pm 0.047	5911 \pm 138

Table 2. **Unconditional Generation on ZINC250k.** Baselines marked with † and ‡ are retrieved from (Wang et al., 2025) and (Wu et al., 2024), respectively. **TIS** (Trajectory Invariance Score) measures latent divergence between isomorphic prefixes (lower is better). SIGMA achieves state-of-the-art FCD among sequence models, effectively bridging the gap with graph-based approaches.

Model	TIS (↓)	Validity (†)	Uniqueness (†)	Novelty (†)	IntDiv (†)	FCD (↓)
<i>Graph-based</i>						
GraphAF†	-	0.685	0.986	-	-	16.02
MoFlow†	-	0.631	0.999	-	-	20.93
LO-ARM†	-	0.961	1.000	-	-	3.229
<i>Sequence-based</i>						
CharRNN‡	-	0.899	0.690	0.182	0.992	0.965
mGPT2‡	-	0.853	0.674	0.672	0.960	0.830
MolGPT‡	-	0.980	0.770	0.766	0.989	0.923
RandSMILES	2.677	0.986	0.756	0.689	0.889	0.892
LTCL	1.698	0.988	0.798	0.711	0.910	0.834
SIGMA (Ours)	0.041	0.998	0.814	0.798	0.910	0.752

ations of local optima), SIGMA leverages its isotropic latent space to facilitate effective **scaffold hopping**. By traversing the connected manifold of isomorphic views, SIGMA avoids syntactic minima, covering a significantly broader chemical space without sacrificing optimization success.

4.4. Breaking the Redundancy Ceiling: Isomorphic Beam Search

We address a decoding bottleneck: standard beam search wastes capacity on redundant isomorphic SMILES. Scaling beam width K from 100 to 50,000 (Fig. 6) shows both methods generate similar numbers of valid SMILES, confirming robust modeling. However, scaffold discovery diverges sharply. Standard beam search saturates near $K = 5,000$, producing mainly redundant variants. **IsoBeam** maintains near-linear growth by pruning isomorphic paths and reallocating computation to distinct regions of chemical space. At $K = 50,000$, IsoBeam finds over **11,000 scaffolds**, roughly $2\times$ the baseline.

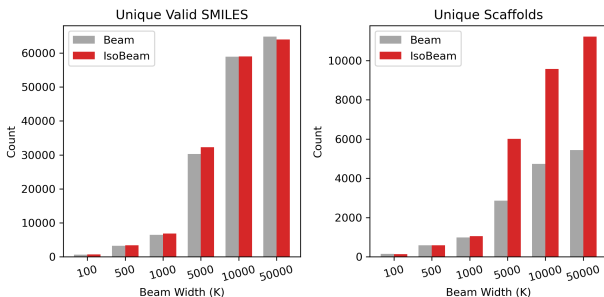


Figure 6. **Inference Scalability Analysis** ($K = 100 \rightarrow 50,000$). **Left:** Both strategies yield comparable valid SMILES, confirming SIGMA’s robustness. **Right:** A critical divergence in scaffold diversity. Standard Beam Search (Grey) saturates at $K \approx 5,000$ due to isomorphic redundancy. In contrast, **IsoBeam** (Red) mines the chemical long-tail, breaking the saturation ceiling to discover $> 2\times$ unique scaffolds at $K = 50,000$.

5. Conclusion

This paper introduces SIGMA, a framework designed to resolve the topological misalignment in autoregressive chemical language models. By enforcing latent isotropy across isomorphic SMILES views, SIGMA effectively eliminates canonicalization bias without relying on computationally expensive graph encoders. Experiments on ZINC-250k show that this geometric regularization effectively bridges the gap with graph-based models, achieving state-of-the-art distributional alignment (FCD) while maintaining superior validity. Furthermore, we show that this invariance is critical for goal-directed optimization, enabling RL agents to explore the chemical space efficiently with significantly reduced mode collapse. These findings suggest that incorporating explicit geometric constraints offers a scalable and robust direction for next-generation molecular generative models.

Impact Statement

Our work aims to advance the field of machine learning for molecular design. The potential societal impact of this research is largely positive, offering tools to accelerate drug discovery and material science. As with any generative technology in chemistry, there is a remote risk of misuse for designing harmful substances. We believe that standard safety protocols in the pharmaceutical industry and responsible release of research code are sufficient to mitigate these risks. We do not foresee any immediate negative societal consequences that require specific highlighting beyond standard dual-use considerations.

References

- Ar-Pous, J., Johansson, S. V., Prykhodko, O., Bjerrum, E. J., Tyrchan, C., Reymond, J.-L., Chen, H., and Engkvist, O. Randomized smiles strings improve the quality of molecular generative models. *Journal of cheminformatics*, 11(1):71, 2019.
- Bagal, V., Aggarwal, R., Vinod, P., and Priyakumar, U. D. Molgpt: molecular generation using a transformer-decoder model. *Journal of chemical information and modeling*, 62(9):2064–2076, 2021.
- Bjerrum, E. J. Smiles enumeration as data augmentation for neural network modeling of molecules. *arXiv preprint arXiv:1703.07076*, 2017.
- Bran, A. M., Cox, S., Schilter, O., Baldassari, C., White, A. D., and Schwaller, P. Chemcrow: Augmenting large-language models with chemistry tools. *arXiv preprint arXiv:2304.05376*, 2023.
- Chithrananda, S., Grand, G., and Ramsundar, B. Chemberta: large-scale self-supervised pretraining for molecular property prediction. *arXiv preprint arXiv:2010.09885*, 2020.
- Devlin, J., Chang, M.-W., Lee, K., and Toutanova, K. Bert: Pre-training of deep bidirectional transformers for language understanding. In *Proceedings of the 2019 conference of the North American chapter of the association for computational linguistics: human language technologies, volume 1 (long and short papers)*, pp. 4171–4186, 2019.
- Fabian, B., Edlich, T., Gaspar, H., Segler, M., Meyers, J., Fiscato, M., and Ahmed, M. Molecular representation learning with language models and domain-relevant auxiliary tasks. *arXiv preprint arXiv:2011.13230*, 2020.
- Ganeeva, V., Sakhovskiy, A., Khrabrov, K., Savchenko, A., Kadurin, A., and Tutubalina, E. Lost in translation: Chemical language models and the misunderstanding of molecule structures. In *Findings of the Association for Computational Linguistics: EMNLP 2024*, pp. 12994–13013, 2024.
- Gao, W., Fu, T., Sun, J., and Coley, C. Sample efficiency matters: a benchmark for practical molecular optimization. *Advances in neural information processing systems*, 35:21342–21357, 2022.
- Gaulton, A., Bellis, L. J., Bento, A. P., Chambers, J., Davies, M., Hersey, A., Light, Y., McGlinchey, S., Michalovich, D., Al-Lazikani, B., et al. ChEMBL: a large-scale bioactivity database for drug discovery. *Nucleic acids research*, 40(D1):D1100–D1107, 2012.
- Gilmer, J., Schoenholz, S. S., Riley, P. F., Vinyals, O., and Dahl, G. E. Neural message passing for quantum chemistry. In *International conference on machine learning*, pp. 1263–1272. Pmlr, 2017.
- Honda, S., Shi, S., and Ueda, H. R. Smiles transformer: Pre-trained molecular fingerprint for low data drug discovery. *arXiv preprint arXiv:1911.04738*, 2019.
- Hu, W., Liu, B., Gomes, J., Zitnik, M., Liang, P., Pande, V., and Leskovec, J. Strategies for pre-training graph neural networks. *arXiv preprint arXiv:1905.12265*, 2019.
- Irwin, J. J. and Shoichet, B. K. Zinc- a free database of commercially available compounds for virtual screening. *Journal of chemical information and modeling*, 45(1): 177–182, 2005.
- Jiang, A., Sablayrolles, A., Roux, A., et al. Mistral 7b. *arXiv preprint arXiv:2310.06825*, 2023.
- Krenn, M., Häse, F., Nigam, A., Friederich, P., and Aspuru-Guzik, A. Self-referencing embedded strings (selfies): A 100% robust molecular string representation. *Machine Learning: Science and Technology*, 1(4):045024, 2020.
- Lee, S., Kreis, K., Veccham, S., Liu, M., Reidenbach, D., Paliwal, S., Vahdat, A., and Nie, W. Molecule generation with fragment retrieval augmentation. *Advances in Neural Information Processing Systems*, 37:132463–132490, 2024.
- Li, Y., Gao, C., Song, X., Wang, X., Xu, Y., and Han, S. Druggpt: a gpt-based strategy for designing potential ligands targeting specific proteins. *bioRxiv*, pp. 2023–06, 2023.
- Liu, Y., Ott, M., Goyal, N., Du, J., Joshi, M., Chen, D., Levy, O., Lewis, M., Zettlemoyer, L., and Stoyanov, V. Roberta: A robustly optimized bert pretraining approach. *arXiv preprint arXiv:1907.11692*, 2019.
- O’Boyle, N. and Dalke, A. Deepsmiles: an adaptation of smiles for use in machine-learning of chemical structures. 2018.

- Olivecrona, M., Blaschke, T., Engkvist, O., and Chen, H. Molecular de-novo design through deep reinforcement learning. *Journal of cheminformatics*, 9(1):48, 2017.
- Pinheiro, G. A., Da Silva, J. L., and Quiles, M. G. Smiclr: Contrastive learning on multiple molecular representations for semisupervised and unsupervised representation learning. *Journal of Chemical Information and Modeling*, 62(17):3948–3960, 2022.
- Qian, Y., Shi, M., and Zhang, Q. Consmi: contrastive learning in the simplified molecular input line entry system helps generate better molecules. *Molecules*, 29(2):495, 2024.
- Radford, A., Wu, J., Child, R., Luan, D., Amodei, D., Sutskever, I., et al. Language models are unsupervised multitask learners. *OpenAI blog*, 1(8):9, 2019.
- Scalia, G., Grambow, C. A., Pernici, B., Li, Y.-P., and Green, W. H. Evaluating scalable uncertainty estimation methods for deep learning-based molecular property prediction. *Journal of chemical information and modeling*, 60(6):2697–2717, 2020.
- Seal, S., Carreras-Puigvert, J., Trapotsi, M.-A., Yang, H., Spjuth, O., and Bender, A. Integrating cell morphology with gene expression and chemical structure to aid mitochondrial toxicity detection. *Communications Biology*, 5(1):858, 2022.
- Seal, S., Yang, H., Trapotsi, M.-A., Singh, S., Carreras-Puigvert, J., Spjuth, O., and Bender, A. Merging bioactivity predictions from cell morphology and chemical fingerprint models using similarity to training data. *Journal of Cheminformatics*, 15(1):56, 2023.
- Shi, C., Xu, M., Zhu, Z., Zhang, W., Zhang, M., and Tang, J. Graphaf: a flow-based autoregressive model for molecular graph generation. *arXiv preprint arXiv:2001.09382*, 2020.
- Sterling, T. and Irwin, J. J. Zinc 15–ligand discovery for everyone. *Journal of chemical information and modeling*, 55(11):2324–2337, 2015.
- Su, Y., Liu, F., Meng, Z., Lan, T., Shu, L., Shareghi, E., and Collier, N. Tacl: Improving bert pre-training with token-aware contrastive learning. *arXiv preprint arXiv:2111.04198*, 2021.
- Tetko, I. V., Karpov, P., Van Deursen, R., and Godin, G. State-of-the-art augmented nlp transformer models for direct and single-step retrosynthesis. *Nature communications*, 11(1):5575, 2020.
- Vaswani, A., Shazeer, N., Parmar, N., Uszkoreit, J., Jones, L., Gomez, A. N., Kaiser, Ł., and Polosukhin, I. Attention is all you need. *Advances in neural information processing systems*, 30, 2017.
- Wang, S., Guo, Y., Wang, Y., Sun, H., and Huang, J. Smilesbert: large scale unsupervised pre-training for molecular property prediction. In *Proceedings of the 10th ACM international conference on bioinformatics, computational biology and health informatics*, pp. 429–436, 2019.
- Wang, Y., Xiao, J., Suzek, T. O., Zhang, J., Wang, J., and Bryant, S. H. Pubchem: a public information system for analyzing bioactivities of small molecules. *Nucleic acids research*, 37(suppl_2):W623–W633, 2009.
- Wang, Y., Wang, J., Cao, Z., and Barati Farimani, A. Molecular contrastive learning of representations via graph neural networks. *Nature Machine Intelligence*, 4(3):279–287, 2022.
- Wang, Z., Shi, J., Heess, N., Gretton, A., and Titsias, M. K. Learning-order autoregressive models with application to molecular graph generation. *arXiv preprint arXiv:2503.05979*, 2025.
- Weininger, D. Smiles, a chemical language and information system. 1. introduction to methodology and encoding rules. *Journal of chemical information and computer sciences*, 28(1):31–36, 1988.
- Wu, J.-N., Wang, T., Chen, Y., Tang, L.-J., Wu, H.-L., and Yu, R.-Q. t-smiles: a fragment-based molecular representation framework for de novo ligand design. *Nature Communications*, 15(1):4993, 2024.
- Xu, L., Xia, L., Pan, S., and Li, Z. Triple generative self-supervised learning method for molecular property prediction. *International Journal of Molecular Sciences*, 25(7):3794, 2024.
- You, J., Liu, B., Ying, Z., Pande, V., and Leskovec, J. Graph convolutional policy network for goal-directed molecular graph generation. *Advances in neural information processing systems*, 31, 2018.
- Zhou, Q., Xu, H., Li, H., Zhang, H., Zhang, X., Wang, Y., and Gao, K. Token-level contrastive learning with modality-aware prompting for multimodal intent recognition. In *Proceedings of the AAAI conference on artificial intelligence*, volume 38, pp. 17114–17122, 2024.
- Zhu, J., Xia, Y., Wu, L., Xie, S., Zhou, W., Qin, T., Li, H., and Liu, T.-Y. Dual-view molecular pre-training. In *Proceedings of the 29th ACM SIGKDD Conference on Knowledge Discovery and Data Mining*, pp. 3615–3627, 2023.

A. Visualization of Trajectory Dynamics

To provide an intuitive understanding of the "manifold fragmentation" problem discussed in Section 4.1 and the redundancy issue addressed in Section 4.4, we visualize the generation trajectories in Figure 7.

Figure 7(b) illustrates the **unconstrained** scenario (characteristic of standard sampling or naive beam search), where the stochastic nature of sequential decoding leads to divergent paths for the same molecular graph. This divergence is the root cause of the "saturation" phenomenon observed in our beam width experiments.

In contrast, Figure 7(c) demonstrates the **constrained** alignment principle. Although visually depicted using randomized training views, this same mechanism underpins our **IsoBeam** decoding strategy: by dynamically recognizing and merging structurally equivalent partial paths (indicated by the converging arrows), the model is forced to explore topologically distinct regions rather than syntactic permutations.

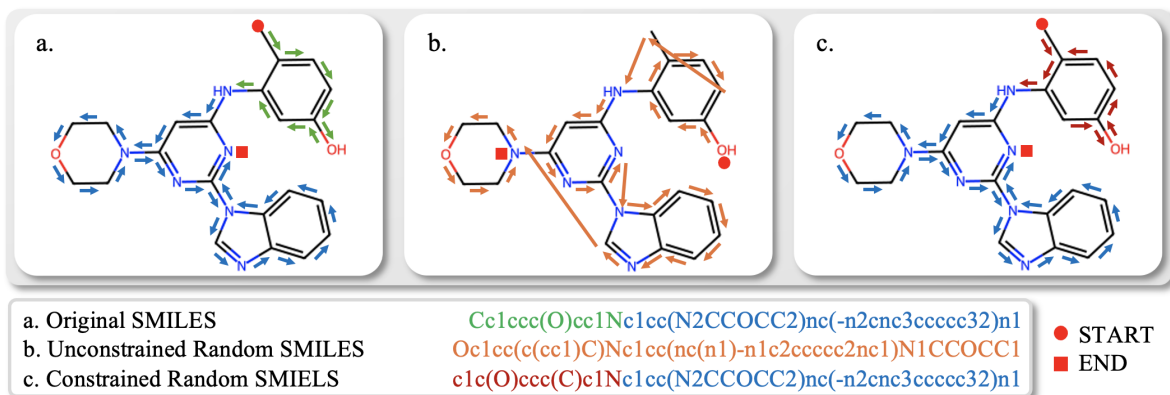


Figure 7. **Conceptual Visualization of Trajectory Dynamics.** (a) The canonical reference path. (b) Unconstrained trajectories diverge into isomorphic variations (Redundancy). (c) Constrained trajectories align structurally equivalent paths. This alignment mechanism is central to SIGMA’s training objective and is explicitly enforced during inference via **IsoBeam** to prune redundant search branches. *Note: START/END markers denote sequence boundaries; arrows indicate traversal direction.

B. Implementation Details

In this section, we provide detailed specifications regarding the model architecture, training hyperparameters, computing infrastructure, and baseline configurations to ensure the reproducibility of our results. Our code and pre-trained models will be made publicly available upon acceptance.

B.1. Model Architecture

We utilize the **GPT-2 Small** architecture as the backbone for the SIGMA model. The model consists of a 12-layer Transformer decoder with 12 attention heads and a hidden dimension of $d_{model} = 768$.

- **Embedding Layer:** We use a learned positional embedding with a maximum sequence length of 128 (covering > 99% of SMILES strings in ZINC-250k).
- **Projection Head:** For the contrastive learning objective (SIGMA alignment), we attach a 2-layer MLP projection head (Hidden dim: 768 \rightarrow 256) to the terminal hidden state of the Transformer. This head is used only during training to compute the contrastive loss and is discarded during inference.
- **Parameter Count:** The total number of trainable parameters is approximately 124M.

B.2. Training Configuration

All models, including SIGMA and sequence-based baselines, were trained for **50 epochs** on the ZINC-250k dataset. We use the AdamW optimizer with a linear learning rate warmup for the first 5% of training steps, followed by a cosine decay schedule. To stabilize training, we apply gradient clipping.

We specifically note that for SIGMA, the batch size refers to the number of unique molecules; since we generate 2 views per molecule for contrastive learning, the effective number of sequences processed per step is $2 \times \text{Batch Size}$.

Detailed hyperparameters are listed in Table 3.

Table 3. Hyperparameter Settings for SIGMA Training.

Hyperparameter	Value
<i>Optimization</i>	
Optimizer	AdamW
Peak Learning Rate	5×10^{-4}
Weight Decay	0.01
Beta parameters	(0.9, 0.999)
Gradient Clipping (Norm)	1.0
Batch Size	64
Training Epochs	50
Warmup Steps	2000
<i>Contrastive Learning</i>	
Temperature (τ)	0.1
Augmentation Views (N)	2
Projection Head Dim	256
<i>Architecture (GPT-2 Small)</i>	
Layers	12
Attention Heads	12
Hidden Dimension	768
Dropout	0.1
Max Sequence Length	128

B.3. Data Preprocessing and Tokenization

- **Dataset:** We use the ZINC-250k dataset (Irwin & Shoichet, 2005), comprising 250,000 commercially available drug-like molecules. We follow the standard random split: 220k for training, 20k for validation, and 10k for testing.
- **Tokenization:** We employ a character-level tokenizer derived from the training set. The vocabulary consists of **69 unique tokens**, including standard atomic symbols (e.g., C, O, N), bond types, branching/ring indicators, and special control tokens (e.g., [BOS], [EOS], [PAD]).
- **Augmentation:** For the contrastive objective, randomized SMILES are generated on-the-fly using RDKit by traversing the molecular graph with random starting atoms and traversal orders.

B.4. Computing Infrastructure

All experiments were conducted on a single **NVIDIA A100 Tensor Core GPU (40GB VRAM)**. The software environment includes:

- **Framework:** PyTorch 2.1.0
- **Chemistry Library:** RDKit 2023.09.5 (for SMILES handling, augmentation, and validity checks).
- **Transformers Library:** HuggingFace Transformers 4.35.0.

Inference with IsoBeam at $K = 50,000$ was optimized using batch processing on the GPU to maximize throughput.

B.5. Inference Details (IsoBeam)

For the asymptotic analysis in Section 4.4, we scaled the beam width K across the set $\{100, 500, 1000, 5000, 10000, 50000\}$.

- **Standard Beam Search:** Implemented using the default HuggingFace `generate` function with `num_beams=K` and `num_return_sequences=K`.
- **IsoBeam:** Implemented as a custom decoding loop. At each step, valid partial SMILES are cached. We utilize a hash map to store InChIKeys of visited structures to perform $O(1)$ redundancy checks.

C. Data Construction and View Generation

To ensure the reproducibility of our topology-aware view construction, we detail the graph partitioning and string generation process utilized in Section 3.2.

C.1. Graph Partitioning Algorithm

For a given molecule $G = (V, E)$, we identify the set of *cuttable bonds* $\mathcal{E}_{cut} \subset E$. A bond $e = (u, v)$ is included in \mathcal{E}_{cut} if and only if:

1. **Acyclicity:** e does not belong to any ring system.
2. **Non-Terminal (Optional):** To avoid creating trivial fragments (e.g., single methyl groups), we typically require that both resulting components have at least **2** heavy atoms.]

During training, for each molecule in a batch, we uniformly sample one bond $e \in \mathcal{E}_{cut}$ to dissolve. This partitions the graph into two connected components: the prefix subgraph G_{pre} and the suffix subgraph G_{suf} .

C.2. Handling Attachment Points

Crucially, simply severing the bond would lose topological information regarding the connection point. To resolve this, we introduce ****dummy atoms**** (anchors) at the cut site.

- The atom u in G_{pre} that was connected to v is marked with a wildcard token (e.g., $*$) or a specific isotope tag to indicate the growth direction.
- This ensures that the SMILES string for G_{pre} explicitly encodes an "open" valency, distinguishing, for example, an ethyl group ($CC*$) from an ethane molecule (CC).

C.3. Contrastive View Generation

The core of SIGMA is strictly aligning syntactically distinct strings that represent the *same* geometric subgraph. Once G_{pre} is fixed:

- **View 1:** We generate a canonical SMILES string $s_{pre}^{(1)}$ of G_{pre} (rooted at the cut point or canonically ordered).
- **View 2:** We generate a randomized SMILES string $s_{pre}^{(2)}$ of the *same* subgraph G_{pre} by performing a random DFS traversal (using RDKit's `doRandom=True`).

This pair $(s_{pre}^{(1)}, s_{pre}^{(2)})$ serves as a positive sample for the contrastive objective, as they are guaranteed to map to the identical topological structure despite their sequence differences.

D. Dense Trajectory Alignment Objective

Given equivalent prefix pairs (p_i, p_j) , SIGMA applies a token-level contrastive objective over their valid suffix trajectories. Let h_t denote the hidden state at position t . We minimize an InfoNCE-style loss:

$$\mathcal{L}_{\text{SIGMA}} = - \sum_t \log \frac{\exp(\text{sim}(h_t^{(i)}, h_t^{(j)})/\tau)}{\sum_k \exp(\text{sim}(h_t^{(i)}, h_t^{(k)})/\tau)}. \quad (8)$$

This aligns representations across equivalent syntactic trajectories, restoring manifold connectivity.

E. Additional Evidence of Geometric Invariance

To verify that the geometric invariance observed in Section 4.1 generalizes to complex pharmaceutical compounds, we conduct an additional microscopic alignment analysis on ****Acetylsalicylic acid (Aspirin)****.

We inspect the attention patterns between two synonymous SMILES representations of Aspirin that differ significantly in their starting syntax:

- **View A:** CC(=O)Oc1ccccc1C(=O)O (Standard canonical start)
- **View B:** O=C(C)Oc1ccccc1C(=O)O (Alternative start with inverted acetyl group)

As visualized in Figure 8, SIGMA exhibits strong ****off-diagonal semantic alignment****. Specifically, the representations of the acetyl group tokens—CC(=O) in View A and O=C(C) in View B—show high cosine similarity (indicated by the bright block in the top-left corner), despite being composed of different character sequences. This confirms that SIGMA has successfully learned to abstract the underlying functional group (the acetyl ester) independent of its specific linearization order. The continued high similarity along the diagonal for the shared benzene ring substructure (Oc1ccccc1...) further validates that the model maintains trajectory consistency once the syntax converges.

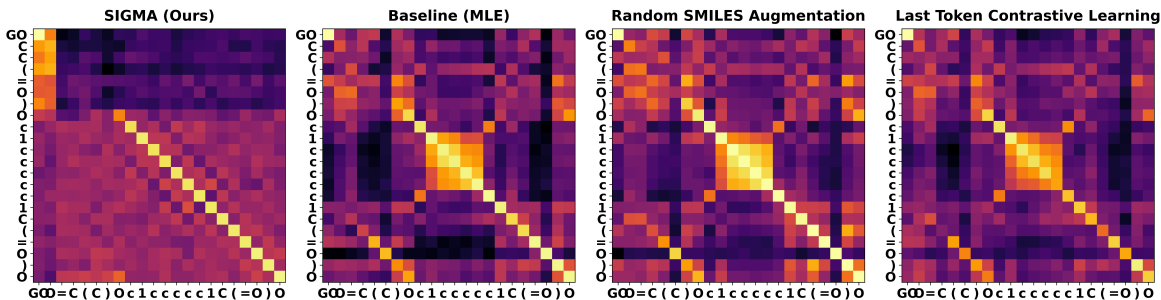


Figure 8. **Geometric Alignment on Acetylsalicylic Acid (Aspirin)**. We visualize the token-level cosine similarity between two isomorphic views of Aspirin: CC(=O)... vs. O=C(C).... The high-similarity region (red block) aligning the distinct prefixes confirms that SIGMA correctly identifies the topological equivalence of the acetyl group despite the variation in linearization direction.

F. Metric Definitions

To ensure reproducibility, we provide formal definitions for all evaluation metrics used in our experiments.

F.1. Generative Quality Metrics

Let \mathcal{G} be the set of generated molecules and \mathcal{D}_{train} be the training dataset.

- **Validity:** The fraction of generated SMILES strings that can be parsed into valid molecular graphs by RDKit.
- **Uniqueness:** The fraction of valid molecules that are unique within the generated set \mathcal{G} .

$$\text{Uniqueness} = \frac{|\text{unique}(\mathcal{G}_{valid})|}{|\mathcal{G}_{valid}|}$$

- **Novelty:** The fraction of valid, unique generated molecules that do not appear in the training set.

$$\text{Novelty} = \frac{|\{m \in \mathcal{G}_{valid} \mid m \notin \mathcal{D}_{train}\}|}{|\mathcal{G}_{valid}|}$$

- **Internal Diversity (IntDiv):** Measures the chemical diversity within the generated set using the average pairwise Tanimoto distance (T_d) of Morgan fingerprints (M).

$$\text{IntDiv}(\mathcal{G}) = 1 - \frac{1}{|\mathcal{G}|^2} \sum_{m_i, m_j \in \mathcal{G}} \text{Tanimoto}(M(m_i), M(m_j))$$

F.2. Distribution Learning Metrics

- **Fréchet ChemNet Distance (FCD):** Measures the distance between the distribution of generated molecules and the test set in the activation space of ChemNet (a pre-trained GRU). Lower FCD indicates that the generated molecules capture the chemical and biological properties of the real data distribution more accurately.
- **Scaffold Diversity (#Scaf):** The number of unique Bemis-Murcko scaffolds extracted from the generated set. A scaffold is obtained by removing all side chain atoms and keeping only the ring systems and linkers. Higher #Scaf indicates better exploration of the structural topology.

F.3. Geometric Invariance Metrics

- **Trajectory Invariance Score (TIS):** A custom metric to quantify the stability of the latent representation against isomorphic permutations. For a given molecule M , let s_1 and s_2 be two distinct SMILES prefixes representing the same partial graph G_{sub} . Let $\mathbf{h}(s)$ denote the normalized terminal hidden state of the model given prefix s . TIS is defined as the expected cosine distance over the test set:

$$\text{TIS} = \mathbb{E}_{M \sim \mathcal{D}_{test}} [1 - \text{sim}(\mathbf{h}(s_1), \mathbf{h}(s_2))]$$

Lower TIS values (closer to 0) indicate stronger geometric invariance, where the model maps syntactically different but topologically equivalent sequences to nearby points in the latent space.

F.4. Optimization Metrics (PMO)

For the Reinforcement Learning tasks, we report:

- **Top-1 / Top-10 / Top-100:** The average reward score of the top K molecules found during the optimization process.
- **Success Rate:** The percentage of generated molecules that satisfy all hard constraints (if applicable) and exceed a predefined reward threshold.